

# M<sub>6</sub>L<sub>12</sub> Nanospheres with Multiple C<sub>70</sub> Binding Sites for <sup>1</sup>O<sub>2</sub> Formation in Organic and Aqueous Media

Eduard O. Bobylev, David A. Poole, III, Bas de Bruin, and Joost N.H. Reek\*



Cite This: *J. Am. Chem. Soc.* 2022, 144, 15633–15642



Read Online

ACCESS |



Metrics & More

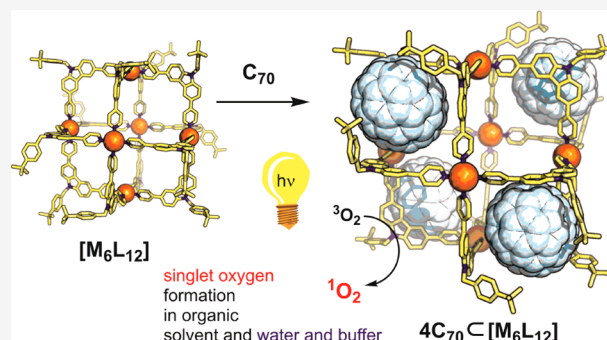


Article Recommendations



Supporting Information

**ABSTRACT:** Singlet oxygen is a potent oxidant with major applications in organic synthesis and medicinal treatment. An efficient way to produce singlet oxygen is the photochemical generation by fullerenes which exhibit ideal thermal and photochemical stability. In this contribution we describe readily accessible M<sub>6</sub>L<sub>12</sub> nanospheres with unique binding sites for fullerenes located at the windows of the nanospheres. Up to four C<sub>70</sub> can be associated with a single nanosphere, presenting an efficient method for fullerene extraction and application. Depending on the functionality located on the outside of the sphere, they act as vehicles for <sup>1</sup>O<sub>2</sub> generation in organic or in aqueous media using white LED light. Excellent productivity in <sup>1</sup>O<sub>2</sub> generation and consecutive oxidation of <sup>1</sup>O<sub>2</sub> acceptors using C<sub>70</sub>C[Pd<sub>6</sub>L<sub>12</sub>], C<sub>60</sub>C[Pd<sub>6</sub>L<sub>12</sub>] or fullerene soot extract was observed. The methodological design principles allow preparation and application of highly effective multifullerene binding spheres.



## INTRODUCTION

Singlet oxygen, an electronically excited form of oxygen, has numerous applications in synthetic chemistry,<sup>1,2</sup> purification,<sup>3</sup> and pharmacology<sup>4–6</sup> due to its strong oxidizing properties.<sup>7</sup> During the last decades, many synthetic protocols were developed based on the reactivity of <sup>1</sup>O<sub>2</sub> with C–H bonds, C=C double bonds, aromatic systems, and heteroatoms (Figure 1).<sup>1</sup> Singlet oxygen finds major application in the clinical photodynamic therapy treatment (PDT) of tumors in which oxidative stress caused by <sup>1</sup>O<sub>2</sub> leads to cell damage or cell death (Figure 1).<sup>6</sup> Generation of singlet oxygen can be achieved via different methods. Apart from stoichiometric chemical reactions, photochemical excitation of an endogenous

photosensitizer and transfer of its excitation energy describe one of the most common methods of <sup>1</sup>O<sub>2</sub> generation (Figure 1). Classically, organic dyes, such as rose bengal or methylene blue, are applied as a photosensitizer.<sup>8,9</sup> Clinical trials using these photosensitizers in PDT are currently pursued;<sup>10</sup> however, these conventional dyes are prone to chemical, photoinduced or enzymatic degradation, limiting their application *in vivo* and lowering their overall efficiency in synthetic chemistry.<sup>11</sup> These major challenges related to PDT can be circumvented using fullerenes, which exhibit ideal stability and good absorbance in the visible light, for photochemical generation of <sup>1</sup>O<sub>2</sub> (Figure 1).<sup>12,13</sup> However, application of fullerenes for *in vivo* <sup>1</sup>O<sub>2</sub> generation or for oxidation reactions for synthetic purposes is often hampered by their poor solubility in most solvents, including water. Therefore, there is an interest in structures that bind fullerene to allow fullerene application in a wide variety of media. Common design features of supramolecular structures that bind fullerene include the use of  $\pi$  surfaces that allow good interaction with the aromatic surface of the fullerene. With that in mind, coordination-based self-assemblies with fullerene

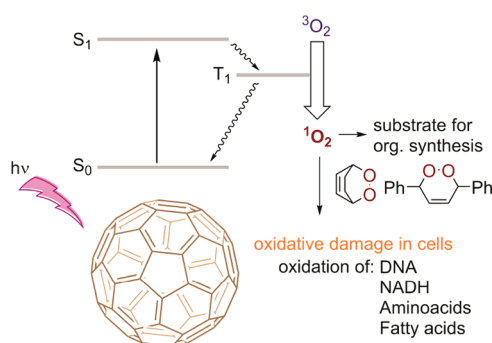


**Figure 1.** Schematic picture of the mechanism of photochemical generation of singlet oxygen by fullerene.

Received: May 29, 2022

Published: August 17, 2022



binding capability can be separated into three different design types (Figure 2). Tweezers are a relatively simple, yet effective

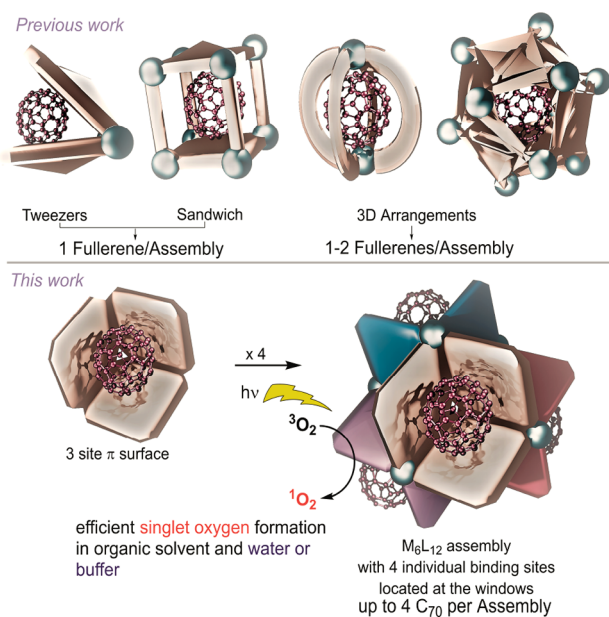


**Figure 2.** Illustration of fullerene binding hosts based on coordination driven self-assembly (top). Design strategy for a multiple-fullerene binding assembly (bottom).

structure for fullerene binding.<sup>14–17</sup> These tweezers typically consist of two aromatic surfaces which are connected by either coordination chemistry or by covalent bonds.

A second type are those with a sandwich type arrangement. Such a structure has two  $\pi$  surfaces, on top and at the bottom, that are connected to one another through different types of linkers.<sup>18–20</sup> The third type consists of three-dimensional cages, capsules, or barrels that surround the fullerene on all sites allowing multiple  $\pi$ -interactions to facilitate binding.<sup>21–29</sup> Most reported spheres bind only 1 fullerene, and only a few examples have been reported in which the host binds multiple fullerene guests.<sup>30–34</sup> Binding multiple fullerenes to a single sphere can not only enhance the fullerene extraction efficiency of the spheres, but can also lead to useful electronic and spectroscopic properties for catalytic applications or preparation of functional materials (such as electron storage devices).<sup>33,35</sup>

To further boost the widespread application of fullerenes, easily accessible and robust structures that effectively bind fullerenes are highly desirable. Here, we present a straightforward strategy to prepare cubic  $M_6L_{12}$  nanospheres that have four independent binding sites for fullerene, which can be readily prepared from commercial materials (Figure 2). We introduce a new design in which fullerene binding occurs at the windows of the self-assembled structure, leading to efficient binding under various conditions. Depending on the structure of the applied building blocks, high binding affinities for fullerenes are realized, leading to novel materials which bear up to four  $C_{70}$  bound to a single nanosphere. The application of functionalized building blocks used for the self-assembly result in nanospheres with various *exo*-functionalization, enabling the binding of fullerene in various organic solvents and even in water. An exploration of their ability to produce  $^1O_2$  in a variety of media and subsequent oxidation of  $^1O_2$  acceptors

revealed high productivity using  $C_{70}C[M_6L_{12}]$  or materials in which fullerenes were directly extracted from fullerene soot using  $[M_6L_{12}]$ . The availability of the herein reported nanospheres together with their ability in  $^1O_2$  generation in various media allow for a more efficient, sustainable application in organic synthesis. The general design principles provide a useful strategy for the construction of novel water-soluble fullerene-binding cages, which are potentially suitable for PDT. With the general simple design principles, we hope to inspire further development of multiple-fullerene binding structures and their widespread applications.

## RESULTS AND DISCUSSION

Inspired by a fullerene binding system developed by Mukherjee and Stang<sup>36</sup> and by square shaped  $Pd_6L_{12}$  nanospheres developed by Fujita,<sup>37</sup> we designed four different building blocks with similar dibenzofuran/carbazole cores. Two of the building blocks  $L^{acetylO}$  and  $L^O$  were chosen in order to study the influence of the rigidity and sphere size on fullerene binding properties (Figure 3). Both are easily

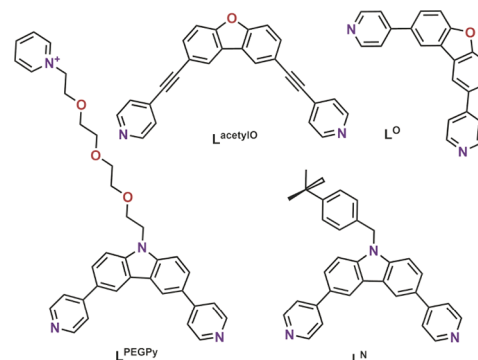


**Figure 3.** Structure of the herein investigated ditopic ligand building blocks used for the preparation of  $Pd_6L_{12}$  nanospheres.

obtained in a one-step procedure via Sonogashira or Suzuki cross-coupling from 2,6-dibromo-dibenzofuran in excellent yields (section S1). Two other types of building blocks were derived from carbazole  $L^N$  and  $L^{PEGPy}$  (Figure 3). Both building blocks ( $L^N$  and  $L^{PEGPy}$ ) are more electron rich, allowing stronger interactions with fullerene.<sup>38–40</sup>  $L^N$  has an extra benzene moiety to potentially increase the  $\pi$ - $\pi$  interactions between the host and the guest and to provide better solubility in organic solvents.  $L^{PEGPy}$  has a hydrophilic group attached to the ligand, making it suitable for the preparation of water-soluble nanospheres. All herein presented ligands have a dihedral angle of  $\sim 90^\circ$  between the pyridine donors and should therefore form  $Pd_6L_{12}$  spheres upon coordination with palladium, as has been shown before for  $L^{acetylO}$  and  $L^O$ .<sup>38,42</sup>

Sphere formation was performed by mixing 1 equiv of  $L^N$  with 0.6 equiv  $[Pd(BF_4)_2(MeCN)_4]$  and 5 mol %  $PdCl_2(MeCN)_2$  as catalyst in dimethyl sulfoxide (DMSO) at  $100^\circ C$  for 24 h according to a previously reported procedure<sup>41</sup> (Figure 4A). After this period, one clear set of protons was observed in the  $^1H$  NMR spectrum of this solution, implying the formation of a highly symmetrical structure (Figure 4C). A downfield shift of the pyridyl protons was observed in accordance to coordination to palladium (signal a and b, Figure 4C). Diffusion ordered NMR (DOSY) displayed one signal corresponding to a hydrodynamic radius of 2 nm in line

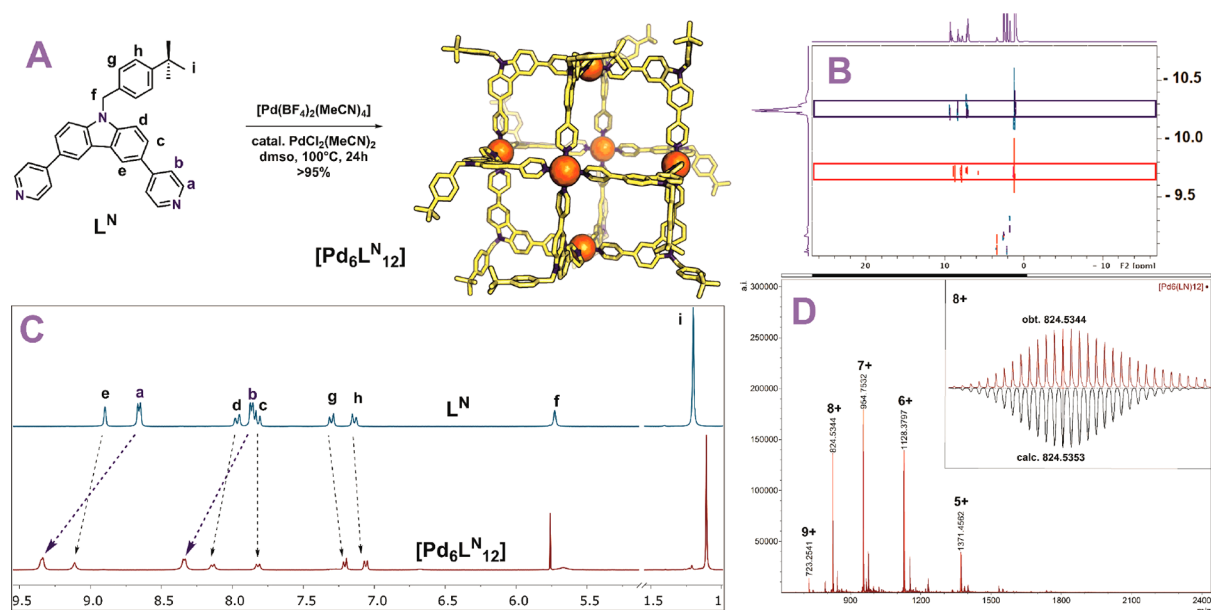


**Figure 4.** Characterization of  $\text{Pd}_6\text{L}^{N}_{12}$ . (A) Reaction conditions for formation of nanospheres. Molecular structure of the displayed sphere was minimized at the PM3 level. Carbon is displayed in yellow, nitrogen in blue, palladium as orange spheres. (B) Overlaid DOSY NMR of the  $[\text{Pd}_6\text{L}^{N}_{12}]$  sphere (blue) and the building block (red). (C)  $^1\text{H}$  NMR spectra of  $[\text{Pd}_6\text{L}^{N}_{12}]$  sphere and the corresponding building block. (D) ESI-MS spectrum of  $[\text{Pd}_6\text{L}^{N}_{12}]$ .

with the formation of  $[\text{Pd}_6\text{L}^{N}_{12}]$  nanosphere (Figure 4B). ESI-MS analysis supported the formation of the desired  $[\text{Pd}_6\text{L}^{N}_{12}]$  sphere, as it displayed only signals corresponding to different charged states of  $[\text{Pd}_6\text{L}^{N}_{12}]^{x+}$  for  $x = 5-9$  (Figure 4D).

All other spheres  $[\text{Pd}_6\text{L}^{\text{acetyIO}}_{12}]$ ,  $[\text{Pd}_6\text{L}^{\text{O}}_{12}]$ , and  $[\text{Pd}_6\text{L}^{\text{PEGPy}}_{12}]$  were obtained by identical experimental procedures to  $[\text{Pd}_6\text{L}^{N}_{12}]$ , featuring all characteristic spectroscopic features similar to  $[\text{Pd}_6\text{L}^{N}_{12}]$  (section S2). All spheres were obtained in excellent yields (>95%, based on  $^1\text{H}$  NMR and MS analysis, section S2) and used as such for subsequent investigations.

**Fullerene Binding Studies.** Fullerene binding experiments were performed by the addition of solid fullerene to DMSO solutions containing the sphere (Figure 5A). The resulting suspensions were stirred at room temperature overnight, filtered, and analyzed by different analytical techniques. Because fullerenes have negligible solubility in DMSO, the presence of characteristic spectroscopic features related to fullerenes can be attributed to binding.

After a mixture of solid  $\text{C}_{60}$  and a solution of  $[\text{Pd}_6\text{L}^{\text{acetyIO}}_{12}]$  nanospheres was stirred, no color change of the solution was observed.  $^1\text{H}$ - and  $^{13}\text{C}$  NMR did not display any difference in the spectra and MS analysis of the solution displayed only signals corresponding to the free  $[\text{Pd}_6\text{L}^{\text{acetyIO}}_{12}]$  nanosphere. Apparently, there is no strong interaction between  $[\text{Pd}_6\text{L}^{\text{acetyIO}}_{12}]$  and fullerene  $\text{C}_{60}$ . Mixing  $\text{C}_{70}$  and  $[\text{Pd}_6\text{L}^{\text{acetyIO}}_{12}]$  also did not change the spectroscopic features, indicating no binding of  $\text{C}_{70}$  either.

Interestingly, mixing solid  $\text{C}_{70}$  with a solution of  $[\text{Pd}_6\text{L}^{\text{O}}_{12}]$ , which is the nanosphere based on a ditopic ligand with only aromatic rings, leads to a color change of the solution from colorless to red-brown. In line with this, an additional absorption was observed in the UV-vis spectrum between 400 and 500 nm, which is characteristic for  $\text{C}_{70}$  (Figure S33).  $^{13}\text{C}$  NMR displayed one new set of signals which can be attributed to  $\text{C}_{70}$ , indicating the presence of  $\text{C}_{70}$  in solution, as a result of binding to  $[\text{Pd}_6\text{L}^{\text{O}}_{12}]$  (Figure S26). ESI-MS analysis

of solutions containing  $[\text{Pd}_6\text{L}^{\text{O}}_{12}]$  and  $\text{C}_{70}$  displayed a range of signals corresponding to host-guest complexes (Figure S31). The most dominant species was attributed to  $(\text{C}_{70})_1\text{C}[\text{Pd}_6\text{L}^{\text{O}}_{12}]$  with a distribution around this main species (Figure 5C). For  $\text{C}_{60}$  and  $[\text{Pd}_6\text{L}^{\text{O}}_{12}]$ , a slight color change was observed (with a weak absorption above 350 nm).  $^{13}\text{C}$  NMR showed the presence of  $\text{C}_{60}$  in solution (Figure S26). Furthermore, ESI-MS analysis displayed a range of signals corresponding to  $\text{C}_{60}\text{C}[\text{Pd}_6\text{L}^{\text{O}}_{12}]$  (Figure S28). Compared to a reaction mixture with  $\text{C}_{70}$  and  $[\text{Pd}_6\text{L}^{\text{O}}_{12}]$ , the spectroscopic features and the peaks in the MS spectra attributed to  $\text{C}_{60}$  bound to  $[\text{Pd}_6\text{L}^{\text{O}}_{12}]$  were less intense, indicating a weaker affinity of the sphere for fullerene  $\text{C}_{60}$  than for  $\text{C}_{70}$ . On the basis of these initial results that suggest stronger binding of fullerenes to nanospheres based on ligand building blocks containing aromatic rings only, that is, the absence of the acetylene bridge between the aromatic units in the building block ( $\text{L}^{\text{acetyIO}}$ ), we next investigated the binding to the nanosphere based on the carbazole building block without any acetylene linkers.

Stirring a mixture of solid  $\text{C}_{70}$  and a DMSO solution of  $[\text{Pd}_6\text{L}^{N}_{12}]$  resulted in a color change from light yellow to dark brown/red. An additional absorption between 400 and 500 nm appeared in the UV-vis spectrum indicative of  $\text{C}_{70}$  binding (Figure S50).  $^{13}\text{C}$  NMR displayed all signals corresponding to the  $[\text{Pd}_6\text{L}^{N}_{12}]$  nanosphere and signals which can be attributed to  $\text{C}_{70}$  (Figure 5B). ESI-MS analysis of the solution displayed multiple species with  $(\text{C}_{70})_4\text{C}[\text{Pd}_6\text{L}^{N}_{12}]$  giving the most pronounced signal with a distribution around this stoichiometry (Figure S46 and Figure 5C). Interestingly, the highest peaks in the MS spectra are those of the host-guest complex with a stoichiometry of 1:4, with only small peaks corresponding to  $(\text{C}_{70})_5\text{C}[\text{Pd}_6\text{L}^{N}_{12}]$ . The nanosphere has in total eight pockets which are available for fullerene binding (Figure 4A, discussion on MS distribution can be found in the Supporting Information, section S8). However, fullerene binding to a pocket withdraws electron density from the

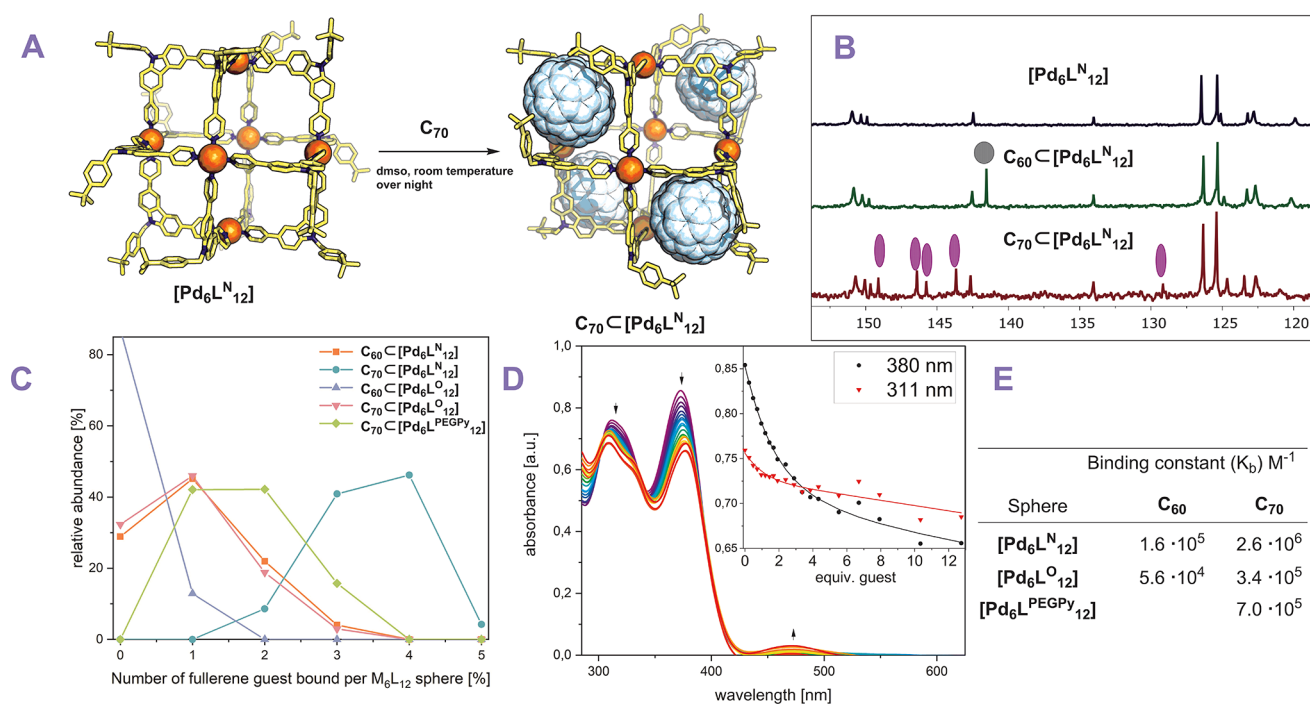


**Figure 5.** Fullerene binding assay of  $Pd_6L_{12}$  nanospheres. (A) Reaction conditions for formation of host–guest complexes. Molecular structure of the displayed assembly was minimized at the PM3 level. Carbon is displayed in yellow, nitrogen in blue, palladium as orange spheres, and fullerene  $C_{70}$  as white spheres. (B)  $^{13}C$  NMR spectra of  $[Pd_6L^N_{12}]$  nanosphere and the corresponding fullerene adducts. (C) Distribution of fullerenes bound to different types of nanospheres based on ESI-MS analysis. (D) Example of an UV–vis titration of  $C_{70}$  to a solution of  $[Pd_6L^N_{12}]$ . Inset: 1:2, H/G binding fit on changes of two different wavelengths. (E) Binding constant of fullerene to different types of spheres obtained by UV–vis titrations.

adjacent aromatic linkers of the nanosphere and possibly bends the linker framework toward the bound fullerene. As a result, the empty pockets adjacent to those that bind a fullerene may therefore bind with lower affinity. Therefore, while the sphere consists of eight binding pockets, it contains only four independent binding pockets (Figure 5A). Our MS experiments show that four binding pockets are occupied by  $C_{70}$  in the  $[Pd_6L^N_{12}]$  nanosphere (as displayed in Figure 5A, the found 1:5 will be discussed later). Interestingly, also mixtures of  $C_{60}$  and  $[Pd_6L^N_{12}]$  displayed a color change to brown.  $^{13}C$  NMR displayed a signal which can be attributed to  $C_{60}$  (Figure 5B). Also, ESI-MS analysis of the solution displayed multiple species with  $(C_{60})_1C[Pd_6L^N_{12}]$  being the most present species (Figure S43 and Figure 5C). The lower amount of  $C_{60}$  associated with  $[Pd_6L^N_{12}]$  (according to ESI-MS analysis, Figure 5C) than  $C_{70}$  indicates a stronger binding for  $C_{70}$  over  $C_{60}$ .

Similar studies using the  $[Pd_6L^{PEGPy}_{12}]$  nanosphere showed that a mixture of host–guest complexes formed, with a different number of  $C_{70}$  bound to the sphere, as judged by the MS data (Figure S56). The species with 1 or 2  $C_{70}$  per nanosphere were dominant as indicated by ESI-MS distribution analysis (Figure 5C). The average number of fullerenes  $C_{70}$  bound to a single  $[Pd_6L^{PEGPy}_{12}]$  sphere is 1.5  $C_{70}$  and is in between the average number of  $C_{70}$  bound to  $[Pd_6L^N_{12}]$  (3.5  $C_{70}$ ) and to  $[Pd_6L^O_{12}]$  (1  $C_{70}$ ) (Figure 5C). These experiments suggest that both the higher electron density and extra aromatic rings on the ditopic ligand building block ( $L^N$ ) located at the building block contribute significantly to better binding of the fullerene guest.

Next to qualitative analysis of the fullerene–sphere host guest complexes using MS analysis, their binding constants were determined by UV–vis titrations (Figure 5E; for details and

elaborate discussion see section S3). Due to the solubility limitation of fullerenes in DMSO, stock solutions of fullerene in toluene were used for these titrations. While the binding may be affected by the presence of toluene, the binding constants obtained provide a relative binding affinity and a lower limit of the binding constant. Upon addition of the  $C_{70}$  (or  $C_{60}$ ) fullerene (in toluene) to a solution of the sphere (in DMSO), changes in the UV–vis spectra are observed. The main absorption corresponding to the spheres (374 nm for  $[Pd_6L^N_{12}]/[Pd_6L^{PEGPy}_{12}]$  and 320 nm for  $[Pd_6L^O_{12}]$ ) decreased, whereas signals associated with the fullerene increased (Figure 5D). As discussed previously,  $Pd_6L_{12}$  nanospheres are multivalent receptors for fullerenes with four independent binding pockets (Figure 5A). As a starting point, we fitted the obtained binding curves of the titration of  $C_{70}$  to  $[Pd_6L^N_{12}]$  using a noncooperative 1:4 or 1:3 model. This gave a binding curve with a large error (20%), a sigmoidal shaped curve and large covariances (Figures S19–S21), implying that a noncooperative 1:4 model is not a good description of the system under diluted UV–vis conditions.<sup>42</sup> As the binding in the presence of toluene as cosolvent may be weaker, we anticipated low contributions of the third and fourth binding at the low concentrations typically used for UV–vis. When we fitted the binding curve in a noncooperative 1:2 model in order to determine the binding strength between  $C_{70}$  and  $[Pd_6L^N_{12}]$ , a better fit was obtained with a lower error (6%) and lower covariances (Figure S23, for elaborate discussion see section S3). Therefore, we employed a 1:2 binding model instead of the 1:4 model for a rough estimation of all binding constants. All binding constants were obtained in good accuracy (error <10%). In agreement with our MS distribution analysis,  $[Pd_6L^N_{12}]$  showed the highest binding constant for  $C_{70}$  ( $2.6 \pm 0.16 \times 10^6 M^{-1}$ ) and  $[Pd_6L^O_{12}]$  binds  $C_{70}$  the weakest ( $3.4 \pm$

$0.19 \times 10^5 \text{ M}^{-1}$ ) (Figure 5E). In line with our MS data,  $[\text{Pd}_6\text{L}^{\text{PEGPy}}_{12}]$  displayed a binding constant for  $\text{C}_{70}$  in between that found for  $[\text{Pd}_6\text{L}^{\text{O}}_{12}]$  and  $[\text{Pd}_6\text{L}^{\text{N}}_{12}]$  ( $7.0 \pm 0.32 \times 10^5 \text{ M}^{-1}$ ). The same trend was found for the binding  $\text{C}_{60}$   $1.6 \pm 0.05 \times 10^5 \text{ M}^{-1}$  for  $[\text{Pd}_6\text{L}^{\text{N}}_{12}]$  and  $5.6 \pm 0.31 \times 10^4 \text{ M}^{-1}$  found for  $[\text{Pd}_6\text{L}^{\text{O}}_{12}]$ . In summary, dibenzofurane and carbazole moieties as part of sphere forming building blocks generate nanospheres that allow fullerene binding. Fully aromatic building blocks show better binding than elongated (acetylene linked) ones. Their binding ability can easily be improved by increasing the electron density of the aromatic group at the building block (carbazole > dibenzofurane). The binding can be further increased by the introduction of extra aromatic moieties on the carbazole nitrogen ( $\text{L}^{\text{N}} > \text{L}^{\text{PEGPy}}$ ).

**Computational Investigation of Binding.** To get further structural insights into the binding stoichiometry of  $\text{C}_{70}$  to  $[\text{Pd}_6\text{L}^{\text{N}}_{12}]$ , we studied the complex *in silico* using molecular dynamics (MD). Our MD models were parametrized following our previously developed protocols.<sup>43</sup> Model environments were constructed to feature  $\text{Pd}_6\text{L}^{\text{N}}_{12}$  and 0–8  $\text{C}_{70}$  positioned randomly within the cage using ProFit.<sup>44</sup> These structures were annealed in explicitly solvated MD simulations (2000 molecules DMSO, 12 molecules  $\text{BF}_4^-$ ) for 50 ns at 300 K. Annealed structures were then optimized, and association enthalpies ( $\Delta H$ ) were estimated by a MMGBSA approach (a technique for estimating the energy of association from energy differences due to host/guest interaction) (Figure 6A, black trace).<sup>45</sup> These simulations showed that  $\text{C}_{70}$  bound preferentially in the windows of  $[\text{Pd}_6\text{L}^{\text{N}}_{12}]$  (Figure 6B) due to the fitting size. While the first  $\text{C}_{70}$  binding is enthalpically unfavorable ( $\Delta H^1 = 1.30 \text{ kcal}\cdot\text{mol}^{-1}$ ), associations of up 2–6  $\text{C}_{70}$  guests is enthalpically

favored with an optimum of four guest molecules per cage ( $\Delta H_4 = -2.48 \text{ kcal}\cdot\text{mol}^{-1}$ ) in line with our HRMS results (Figure 6A, red trace). This preference for multiple guest binding (2–6  $\text{C}_{70}$ ) arises from favorable guest–guest interactions ( $\pi$ – $\pi$  stacking) within the capsule. When 3–4 fullerenes are associated with the windows of a sphere, a  $\pi$ -rich binding site is created on the interior space of the sphere, facilitating the further association of a fifth  $\text{C}_{70}$  (Figure 6C, Figure S45). We anticipate this  $\pi$ -rich environment may facilitate the encapsulation of guest substrate molecules as a biomimetic active site, benefiting photocatalytic applications (see discussion S10). These calculations provide a good explanation why we observe mostly a 4:1 complex by ESI-MS from samples in which the fullerene was extracted using nanosphere solutions in DMSO. As the binding constants were obtained from titration experiments carried out in toluene–DMSO mixtures, quantitative comparison of these data is difficult.

**Photocatalytic Formation of  $^1\text{O}_2$ .** Although fullerenes have ideal photostability and efficiency in  $^1\text{O}_2$  generation, their broad applicability in singlet oxygen generation is limited due to their limited solubility (Table 1, right). Typically, only

**Table 1. Oxidation of Organic  $^1\text{O}_2$  Acceptors by Light Induced Singlet Oxygen Formation in Different Media**

Polarity	#	Solvent	Encapsulated Fullerene Catalyst <sup>a</sup>	Conversion (TON) <sup>b</sup>	free $\text{C}_{70}$ <sup>d</sup>
↓	1	$\text{C}_6\text{H}_6$	$\text{C}_{70}\text{C}\text{Pd}_6\text{L}^{\text{N}}_{12}$	85% (4100)	95%
	2	$\text{CHCl}_3$	$\text{C}_{70}\text{C}\text{Pd}_6\text{L}^{\text{N}}_{12}$	95% (4600)	95%
	3	Acetone	$\text{C}_{70}\text{C}\text{Pd}_6\text{L}^{\text{N}}_{12}$	52% (2500)	5%
	4	MeCN	$\text{C}_{70}\text{C}\text{Pd}_6\text{L}^{\text{N}}_{12}$	70% (3400)	5%
	5	DMF	$\text{C}_{70}\text{C}\text{Pd}_6\text{L}^{\text{N}}_{12}$	70% (3400)	60%
	6 <sup>c</sup>	MeOD	$\text{C}_{70}\text{C}\text{Pd}_6\text{L}^{\text{PEGPy}}_{12}$	67% (3200)	0% <sup>c</sup>
	7 <sup>c</sup>	$\text{D}_2\text{O}$	$\text{C}_{70}\text{C}\text{Pd}_6\text{L}^{\text{PEGPy}}_{12}$	66% (3200)	0% <sup>c</sup>

<sup>a</sup>Standard condition: sphere, 4.16 nmol, substrate 20  $\mu\text{mol}$  in 1 mL solvent, 4 h, room temperature; reactions performed in quartz containers located 2 cm away from a white LED light source. <sup>b</sup>Conversion and turnover number (TON) based on nanosphere amount was determined by  $^1\text{H}$  NMR using mesitylene as internal standard. <sup>c</sup>*N*-(*tert*-Butoxycarbonyl)-L-methionine (20  $\mu\text{mol}$ ) was used as substrate. <sup>d</sup> $\text{C}_{70}$  16.6 nmol dissolved in 10  $\mu\text{L}$  of toluene and 1 mL of cosolvent (described in the table). <sup>e</sup>Free  $\text{C}_{70}$  was added as a solid.

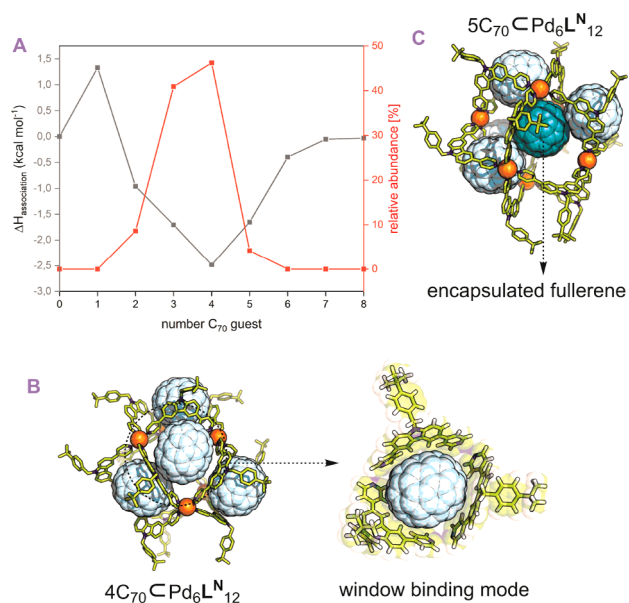


**Figure 6.** Computational investigation on  $\text{C}_{70}$  binding of  $[\text{Pd}_6\text{L}^{\text{N}}_{12}]$  using molecular dynamics (MD). (A) Display of averaged total association enthalpies for different amount of  $\text{C}_{70}$  bound to a single sphere and the obtained distribution of  $\text{C}_{70}$  associated with  $[\text{Pd}_6\text{L}^{\text{N}}_{12}]$  using the MS analysis. (B) Optimized structure of four  $\text{C}_{70}$  associated with a single sphere, displaying the window binding motif. (C) Optimized structure of five  $\text{C}_{70}$  associated with a single sphere, displaying the creation of a hydrophobic interior binding site for the fifth  $\text{C}_{70}$ .

rather apolar solvents such as benzene and chloroform allow for sufficient concentrations of fullerene. Therefore, substrates which do not dissolve in these rather apolar solvents cannot be efficiently oxidized using fullerene-mediated photogenerated  $^1\text{O}_2$ . To extend the application of fullerenes to water and polar solvents, which are generally suitable for many organic compounds and materials, fullerene-binding spheres can act as vehicles which allow solubility in these solvents. Given the strong binding between the fully aromatic spheres  $[\text{Pd}_6\text{L}^{\text{N}}_{12}]$ ,  $[\text{Pd}_6\text{L}^{\text{O}}_{12}]$ , and  $[\text{Pd}_6\text{L}^{\text{PEGPy}}_{12}]$  with fullerenes, their application in singlet oxygen generation in different solvents and consecutive oxidation of model substrates was studied. First, the conversion of anthracene (which is a well-known aromatic

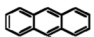
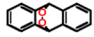
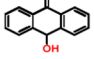
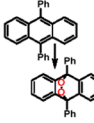
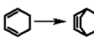
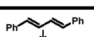
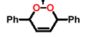
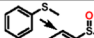
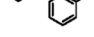
singlet oxygen acceptor) was studied (Table 1, entry 1–5). In the absence of any photosensitizer, irradiation of a solution containing anthracene with white LED light showed no conversion, showing that there is no background reaction. We started the photocatalytic  $^1\text{O}_2$  based reactions using fullerene  $\text{C}_{70}$  (as it has a higher visible light absorbance than  $\text{C}_{60}$ ) bound to various cages in different solvents. The solvent compatibility using  $\text{C}_{70}\text{C}[\text{Pd}_6\text{L}^{\text{N}}_{12}]$  was explored and compared to experiments in which the free  $\text{C}_{70}$  was used (Table 1). As expected, in benzene and chloroform both free  $\text{C}_{70}$  and using  $\text{C}_{70}\text{C}[\text{Pd}_6\text{L}^{\text{N}}_{12}]$  acted as good photocatalyst, and there was hardly any difference in conversion (entry 1 and 2). In contrast, the  $\text{C}_{70}\text{C}[\text{Pd}_6\text{L}^{\text{N}}_{12}]$  system showed to be an excellent candidate for  $^1\text{O}_2$  generation and consecutive oxidation of anthracene in more polar organic solvents, including acetone, acetonitrile, and dimethylformamide, and in these solvents the free  $\text{C}_{70}$  resulted typically in low yields. Because free  $\text{C}_{70}$  displayed good activity in apolar solvents, the enhanced activity of the sphere-fullerene complex in comparison to free  $\text{C}_{70}$  in polar solvents can mainly be attributed to the enhanced solubility (discussion on other effects can be found in section S10). Reactions in polar solvents using  $\text{C}_{70}\text{C}[\text{Pd}_6\text{L}^{\text{N}}_{12}]$  system resulted in high yields and turn over number (TON > 2000, Table 1, entries 3–5).

After demonstrating that the  $\text{C}_{70}$  containing the  $[\text{Pd}_6\text{L}^{\text{N}}_{12}]$  nanosphere displays a high productivity in light driven  $^1\text{O}_2$  in organic medium, we further expanded the scope by introducing the nanosphere–fullerene assemblies into more polar and aqueous media. For the application in water, the solubility of the nanosphere and the host–guest complex was achieved by using hydrophilic side chains attached to the outside of the sphere  $[\text{Pd}_6\text{L}^{\text{PEGPy}}_{12}]$ . Boc-methionine, a well-known  $^1\text{O}_2$  acceptor was applied as the substrate in these polar solvents since anthracene is insufficiently soluble in water and polar solvents.  $\text{C}_{70}\text{C}[\text{Pd}_6\text{L}^{\text{PEGPy}}_{12}]$  showed good productivity in aqueous media (TON = 3200, Table 1, entry 7, solubility assessment S11), making it a suitable candidate for  $^1\text{O}_2$  generation in water, enhancing significantly the applicability scope of fullerenes. As free  $\text{C}_{70}$  does not dissolve, experiments using free  $\text{C}_{70}$  as catalysts resulted in no conversion at all.

**Substrate Scope and Soot Extract Photocatalytic  $^1\text{O}_2$  Formation.** After having established the solvent compatibility of the  $\text{C}_{70}\text{C}$ sphere complex, acetonitrile was chosen as standard solvent for productivity and scope investigation of all developed systems. Interestingly, under these conditions the  $[\text{Pd}_6\text{L}^{\text{N}}_{12}]$  nanospheres themselves showed some catalytic productivity in the peroxidation of anthracene. Whereas  $[\text{Pd}_6\text{L}^{\text{O}}_{12}]$  showed a marginal productivity (TON = 20), which is attributed to the background reaction,  $[\text{Pd}_6\text{L}^{\text{N}}_{12}]$  showed to be a good photocatalyst for the peroxidation of anthracene (TON = 630). We attribute the catalytic productivity of  $[\text{Pd}_6\text{L}^{\text{N}}_{12}]$  to the weak absorption of the nanosphere above 400 nm (Figure 5D), which is an excitation wavelength of the carbazole unit of the building block, which is part of the nanosphere (for comparison with other systems, see for example, refs 46–48).  $[\text{Pd}_6\text{L}^{\text{O}}_{12}]$  has no absorption above 400 nm, making the sphere itself less effective in  $^1\text{O}_2$  generation using white LED light.

In line with the better absorbance of  $\text{C}_{70}$  than  $\text{C}_{60}$  in the visible light, higher productivity was obtained using  $\text{C}_{70}\text{C}[\text{Pd}_6\text{L}^{\text{N}}_{12}]$  than  $\text{C}_{60}\text{C}[\text{Pd}_6\text{L}^{\text{N}}_{12}]$  (Table 2, entries 4 and 5). Also directly extracted fullerene from fullerene soot (as produced by arc vaporization)<sup>49</sup> using  $[\text{Pd}_6\text{L}^{\text{N}}_{12}]$  was applied

**Table 2. Oxidation of Organic Substrates by Light Induced Singlet Oxygen Formation**

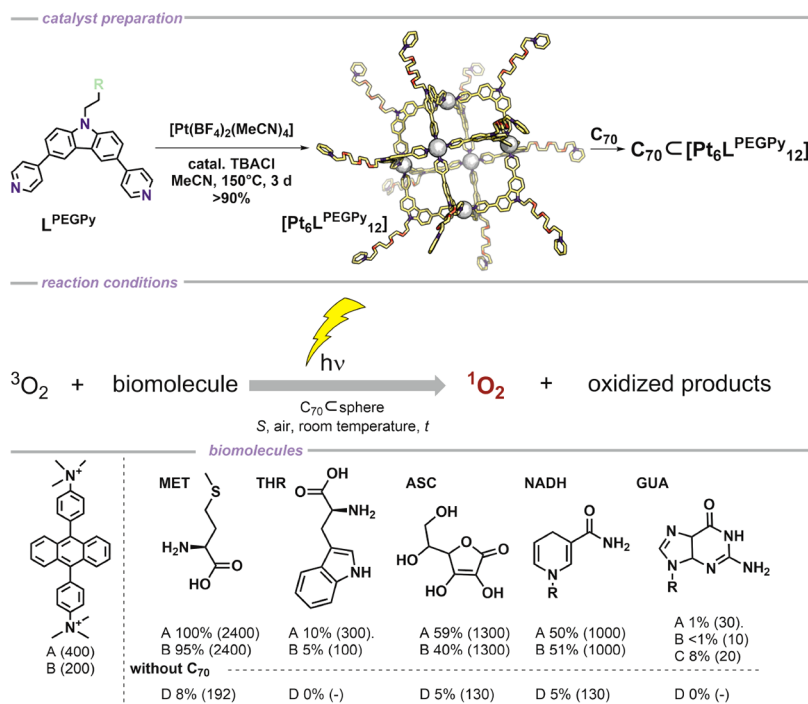
Substrate/Product	#	Catalyst <sup>a</sup>	TON per sphere <sup>b</sup>	Conversion [%]
	1	None	0	0
	2	$\text{Pd}_6\text{L}^{\text{N}}_{12}$	630	26
	3	$\text{Pd}_6\text{L}^{\text{O}}_{12}$	20	1
	4	$\text{C}_{60}\text{C}[\text{Pd}_6\text{L}^{\text{N}}_{12}]$	1200	50
	5*	$\text{C}_{70}\text{C}[\text{Pd}_6\text{L}^{\text{N}}_{12}]$	3400	70
	6	$\text{C}_{60}/\text{C}_{70}^{\text{soot}}\text{C}[\text{Pd}_6\text{L}^{\text{N}}_{12}]$	1400 <sup>c</sup>	58
	7	$\text{C}_{70}\text{C}[\text{Pd}_6\text{L}^{\text{O}}_{12}]$	430	18
	8*	$\text{C}_{70}\text{C}[\text{Pd}_6\text{L}^{\text{N}}_{12}]$	3200	67
	9	$\text{C}_{60}/\text{C}_{70}^{\text{soot}}\text{C}[\text{Pd}_6\text{L}^{\text{N}}_{12}]$	900	37
	10*	$\text{C}_{70}\text{C}[\text{Pd}_6\text{L}^{\text{N}}_{12}]$	2400	75
	11	$\text{C}_{60}/\text{C}_{70}^{\text{soot}}\text{C}[\text{Pd}_6\text{L}^{\text{N}}_{12}]$	800	73
	12*	$\text{C}_{70}\text{C}[\text{Pd}_6\text{L}^{\text{N}}_{12}]$	1400	30
	13	$\text{C}_{60}/\text{C}_{70}^{\text{soot}}\text{C}[\text{Pd}_6\text{L}^{\text{N}}_{12}]$	300	13
	14*	$\text{C}_{70}\text{C}[\text{Pd}_6\text{L}^{\text{N}}_{12}]$	1100, 2400 <sup>d</sup>	15 (50 <sup>d</sup> )
	15*	$\text{C}_{60}/\text{C}_{70}^{\text{soot}}\text{C}[\text{Pd}_6\text{L}^{\text{N}}_{12}]$	50, 380 <sup>d</sup>	1 (8 <sup>d</sup> )

<sup>a</sup>Standard condition: Sphere 4.16 nmol, Substrate 10  $\mu\text{mol}$  (\* 20  $\mu\text{mol}$  of substrate was used instead as full conversion was reached with 10  $\mu\text{mol}$ ) in 1 mL MeCN- $d_3$ , 4 h, room temperature; reactions performed in quartz containers located 2 cm away from a white LED light source. <sup>b</sup>Turnover number (TON) based on nanosphere amount was determined by  $^1\text{H}$  NMR using mesitylene as internal standard. <sup>c</sup>10-hydroxyanthracen-9(10H)-one was identified as the main product.

in catalysis. Fullerene directly extracted from fullerene soot is economically preferred due to its large availability (for the procedure, see experimental section). The MS-analysis of  $\text{C}_{60}/\text{C}_{70}^{\text{soot}}\text{C}[\text{Pd}_6\text{L}^{\text{N}}_{12}]$  displayed a range of fullerene-sphere adducts (Figure S48). The major species were attributed to  $\text{C}_{60}\text{C}[\text{Pd}_6\text{L}^{\text{N}}_{12}]$ ,  $\text{C}_{70}\text{C}[\text{Pd}_6\text{L}^{\text{N}}_{12}]$ , and to mixtures of both fullerenes associated with the nanosphere (see section S5 for details of soot extraction). The  $\text{C}_{60}/\text{C}_{70}^{\text{soot}}\text{C}[\text{Pd}_6\text{L}^{\text{N}}_{12}]$  complex displayed good catalytic productivity (TON = 1400), exceeding the performance of pure  $\text{C}_{60}\text{C}[\text{Pd}_6\text{L}^{\text{N}}_{12}]$ . Since  $\text{C}_{70}$  outperforms  $\text{C}_{60}$ , the soot extract which is a mixture of both fullerenes outperforms pure  $\text{C}_{60}\text{C}[\text{Pd}_6\text{L}^{\text{N}}_{12}]$ , but performs less well than pure  $\text{C}_{70}\text{C}[\text{Pd}_6\text{L}^{\text{N}}_{12}]$ . Interestingly, the  $\text{C}_{60}/\text{C}_{70}^{\text{soot}}\text{C}[\text{Pd}_6\text{L}^{\text{N}}_{12}]$  composite yields a different product than all other applied catalysts (Table 2, entry 6).

The dibenzofurane based structures  $\text{C}_{70}\text{C}[\text{Pd}_6\text{L}^{\text{O}}_{12}]$  performed less well than all other applied catalysts. This can be attributed to a lack of visible absorption of  $\text{L}^{\text{O}}$  and the lower amount of  $\text{C}_{70}$  bound to  $[\text{Pd}_6\text{L}^{\text{O}}_{12}]$  (Table 2, entry 7).

Both  $\text{C}_{70}\text{C}[\text{Pd}_6\text{L}^{\text{N}}_{12}]$  and  $\text{C}_{60}/\text{C}_{70}^{\text{soot}}\text{C}[\text{Pd}_6\text{L}^{\text{N}}_{12}]$  were studied in a small scope of substrates. For diphenyl anthracene,  $\text{C}_{60}/\text{C}_{70}^{\text{soot}}\text{C}[\text{Pd}_6\text{L}^{\text{N}}_{12}]$  and  $\text{C}_{70}\text{C}[\text{Pd}_6\text{L}^{\text{N}}_{12}]$  displayed a similar activity as found for anthracene (Table 2, entries 8 and 9). Cyclohexadiene was converted slightly less efficiently, and it resulted in the formation of different products. The major

Scheme 1. Oxidation of Biomolecules by Light Induced Singlet Oxygen Formation in Aqueous Media<sup>a</sup>

<sup>a</sup>Top:  $[\text{Pt}_6\text{L}^{\text{PEGPy}}]_{12}$  sphere formation procedure and  $\text{C}_{70}$  incorporation. Bottom: Standard reaction condition for oxidation of biomolecules using  $\text{C}_{70}\text{C}[\text{Pt}_6\text{L}^{\text{PEGPy}}]_{12}$ : (A)  $\text{C}_{70}\text{C}[\text{Pt}_6\text{L}^{\text{PEGPy}}]_{12}$  4.16 nmol, substrate 10  $\mu\text{mol}$  in 1 mL of  $\text{D}_2\text{O}$  and 5  $\mu\text{L}$  of DMSO (0.5%), 4 h, room temperature, white 11W LED. Deviation from standard reaction conditions: (B) reaction performed in 0.5 mL of  $\text{D}_2\text{O}$  and 0.5 mL of (1 N)  $\text{PBS}_{\text{aq}}$ ; (C)  $\text{C}_{70}\text{C}[\text{Pt}_6\text{L}^{\text{PEGPy}}]_{12}$  41.6 nmol. Turnover number (TON) and conversion were determined by  $^1\text{H}$  NMR using maleic acid as internal standard. (D) Empty  $[\text{Pt}_6\text{L}^{\text{PEGPy}}]_{12}$  4.16 nmol used as a catalyst in 0.5 mL of  $\text{D}_2\text{O}$  and 0.5 mL of (1 N)  $\text{PBS}_{\text{aq}}$ .

species was identified as the expected peroxy species and minor amounts of aldehydes were formed as judged by  $^1\text{H}$  NMR spectra (Figure S69). Acyclic alkenes were oxidized by both  $\text{C}_{70}\text{C}[\text{Pd}_6\text{L}^{\text{N}}]_{12}$  and  $\text{C}_{60}/\text{C}_{70}^{\text{soot}}\text{C}[\text{Pd}_6\text{L}^{\text{N}}]_{12}$  with lower productivity compared to the previous substrates. Interestingly, also the challenging oxidation of thioanisole was possible using  $\text{C}_{70}\text{C}[\text{Pd}_6\text{L}^{\text{N}}]_{12}$  or  $\text{C}_{60}/\text{C}_{70}^{\text{soot}}\text{C}[\text{Pd}_6\text{L}^{\text{N}}]_{12}$  with good conversion after 8 h, whereas in the absence of nanospheres no conversion of the product was observed. In short, the fullerene containing  $\text{Pd}_6\text{L}_{12}$  nanospheres are readily available and yield systems that are effective in  $^1\text{O}_2$  generation for the application in oxidation of aromatics, cyclic- and acyclic dienes, and thioethers with turnovers of 300–3400. The spheres can be easily separated from the desired products by either column chromatography or precipitation, making them useful candidates for application in organic synthesis.

**Catalytic Formation of  $^1\text{O}_2$  in Water and Buffer.** As mentioned in the introduction, a major  $^1\text{O}_2$  application field is photodynamic therapy. After supporting the effectiveness of our design to bind efficiently multiple fullerenes and displaying activity in  $^1\text{O}_2$  production using palladium-based spheres in organic or aqueous medium, we further expanded the applicability scope by introducing the nanospheres into biologically relevant conditions. For the application in biological medium, solubility in aqueous buffer and good stability against biologically relevant molecules (such as chloride, amines, and acids) is required. As demonstrated before, palladium based nanospheres were shown to be not sufficiently stable under these circumstances.<sup>50</sup> Generally, the platinum counterparts of  $\text{M}_n\text{L}_{2n}$  nanospheres exhibit improved stability under biologically relevant conditions and have

fluorescent properties.<sup>50–53</sup> Platinum-based sphere formation was performed according to reported protocols.<sup>41,50,53,54</sup> The nanosphere was prepared by mixing 0.6 equiv  $[\text{Pt}(\text{BF}_4)_2(\text{MeCN})_4]$ , 7 mol % TBACl as catalyst, and 1 equiv  $\text{L}^{\text{PEGPy}}$  in acetonitrile at 150 °C for 72 h (Scheme 1). After this period a clear downfield shift of the pyridine protons together with a lower diffusion coefficient in DOSY NMR supported the formation of the desired  $[\text{Pt}_6\text{L}^{\text{PEGPy}}]_{12}$  nanosphere (Figures S90–S93). A detailed analysis of the recorded MS spectrum revealed a good selectivity for the formation of  $[\text{Pt}_6\text{L}^{\text{PEGPy}}]_{12}$ . The major species found in the MS analysis were attributed to different charge states of  $[\text{Pt}_6\text{L}^{\text{PEGPy}}]_{12}^{x+}$  for  $x = 4–12$  (Figure S93). Minor amounts of  $[\text{Pt}_3\text{L}^{\text{PEGPy}}]_{10}$  were also detected, giving an overall 90% selectivity for the desired  $[\text{Pt}_6\text{L}^{\text{PEGPy}}]_{12}$  nanosphere based on MS analysis (for quantification see ref 54). The nanosphere showed similar binding features for  $\text{C}_{70}$  as the corresponding palladium counterpart, making it a suitable candidate for further investigation (Figure S95).

First, the stability of  $[\text{Pd}_6\text{L}^{\text{PEGPy}}]_{12}$  and  $[\text{Pt}_6\text{L}^{\text{PEGPy}}]_{12}$  was briefly studied. In agreement with previous reports,  $[\text{Pd}_6\text{L}^{\text{PEGPy}}]_{12}$  decomposed quickly after being exposed to  $\text{NaCl}_{\text{aq}}$  as evidenced by formation of a precipitate and the disappearance of the sphere associated signals in  $^1\text{H}$  NMR.  $[\text{Pt}_6\text{L}^{\text{PEGPy}}]_{12}$  remained in solution after 10 h at 37 °C. No precipitate was formed, and all signals associated with the nanosphere remained the same in the  $^1\text{H}$  NMR spectrum during the course of the experiment (Figure S97).  $[\text{Pt}_6\text{L}^{\text{PEGPy}}]_{12}$  displays emission around 450 nm when excited at 380 nm (Figure S98). In agreement to previous investigations on fullerene binding self-assemblies, the fluorescence is quenched to a certain degree when fullerene

is bound (Figure S98). With the promising fluorescence and stability of  $[\text{Pt}_6\text{L}^{\text{PEGPy}}_{12}]$ , its application in  $^1\text{O}_2$  generation in aqueous media was studied. We decided to investigate the  $^1\text{O}_2$  formation ability by employing a variety of well-known  $^1\text{O}_2$  quenchers which can be found in living cells under two different conditions. Previous investigations into  $^1\text{O}_2$  reactivity in living cells identified the major absorbents being proteins (40%), ascorbate (15%), water (7%), and NADPH (1%).<sup>55</sup> Therefore, we studied some of the most common quenchers using our  $^1\text{O}_2$  generating assembly. We investigated the productivity of  $\text{C}_{70}\text{C}[\text{Pt}_6\text{L}^{\text{PEGPy}}_{12}]$  using a white 11 W LED as source in (A)  $\text{D}_2\text{O}$ , (B) PBS buffered water (Scheme 1).

The generation of  $^1\text{O}_2$  in aqueous medium and in buffered solution upon irradiation with white LED light is supported by the oxidation of substituted anthracene (Scheme 1). Next, different types of amino acids, as model substrates for proteins, were applied as substrates for light driven oxidation.  $\text{C}_{70}\text{C}[\text{Pt}_6\text{L}^{\text{PEGPy}}_{12}]$  promotes oxidation of methionine and tryptophan in  $\text{D}_2\text{O}$  using white LED light (Scheme 1, condition A, TON = 100–2400). Similar results are also obtained when PBS buffered water is used as the reaction medium (Scheme 1, condition B). Because oxidation is not promoted when no fullerene-carrier is applied, this observation supports a good stability of complexes in the presence of chloride and amines. In comparison to the fullerene loaded nanosphere, control experiments with the empty  $[\text{Pt}_6\text{L}^{\text{PEGPy}}_{12}]$  nanosphere show also formation of  $^1\text{O}_2$  but to a much lesser extent (Scheme 1; condition D, for example, 8% for methionine in the absence of fullerene (D) and 95% in the presence (B)). Common biologically relevant reductants such as NADH and ascorbate are oxidized successfully with similar turnovers (around 1000) using either of the two reaction conditions. Finally, also guanosine was briefly studied. Using white light in water (condition A) or in PBS (condition B) affords little conversion of the starting material (~1%). Increasing the catalyst loading by 10-fold (condition C) increases the conversion accordingly to 8%. Whereas the conversions are not very high, it is important to mention that the individual nanospheres reach a turnover of 10–30 in the oxidation of guanosine, which makes them potentially efficient candidates for damaging DNA.

Although a brief study into biologically relevant application, we showed that  $\text{C}_{70}\text{C}[\text{Pt}_6\text{L}^{\text{PEGPy}}_{12}]$  is productive in  $^1\text{O}_2$  generation in aqueous and buffered solutions. Different types of prominent  $^1\text{O}_2$  acceptors such as amino acids and reducing agents were oxidized in PBS using white LED light, making  $[\text{Pt}_6\text{L}^{\text{PEGPy}}_{12}]$  a potential vehicle for fullerene application for further investigations into the biomedical fields.

## CONCLUSION

We introduced new  $\text{M}_6\text{L}_{12}$  nanospheres that can bind fullerenes to the windows of these cubic self-assembled structures. This is a new design principle for fullerene binding as previous structures allowed binding to the interior space. Utilizing the window space allowed the  $\text{M}_6\text{L}_{12}$  spheres to carry up to four fullerenes. The  $\text{M}_6\text{L}_{12}$  nanospheres rely on a simple ligand design and are readily available from commercial materials. The  $\text{Pd}_6\text{L}_{12}$  nanospheres were shown to bind fullerene after extraction from soot. The fullerenes containing  $\text{Pd}_6\text{L}_{12}$  nanospheres are productive in light driven  $^1\text{O}_2$  formation which can be used for the oxidation of a variety of organic compounds in organic solvents of different polarity. Exploiting the easy derivatization of the building blocks used

for  $\text{Pd}_6\text{L}_{12}$  nanospheres formation, allowed the preparation of a water-soluble fullerene-containing nanospheres. This  $[\text{Pd}_6\text{L}^{\text{PEGPy}}_{12}]$  nanosphere is active in the generation of  $^1\text{O}_2$  in water, and as such can be used in catalytic oxidation. The biological relevance of the application of  $\text{C}_{70}\text{C}[\text{Pt}_6\text{L}^{\text{PEGPy}}_{12}]$  in  $^1\text{O}_2$  generation in aqueous and buffered solutions is briefly demonstrated by the light driven oxidation of some amino acids and reducing agents in PBS using white LED light. This makes  $[\text{Pt}_6\text{L}^{\text{PEGPy}}_{12}]$  a potential vehicle for fullerene application in the biomedical fields, which deserves further investigation. The general design principle and the ease of derivatization of the building blocks for cage formation provide a strong basis for the design of systems suitable for PDT, an avenue that is currently be further explored. This work provides new design strategies for the development of efficient and active fullerene binding coordination-based  $\text{M}_6\text{L}_{12}$  nanospheres.

## ASSOCIATED CONTENT

### Supporting Information

The Supporting Information is available free of charge at <https://pubs.acs.org/doi/10.1021/jacs.2c05507>.

NMR spectra for all compounds, mass spectrometry, synthetic and additional experimental details and methods (PDF)

## AUTHOR INFORMATION

### Corresponding Author

Joost N.H. Reek – van 't Hoff Institute for Molecular Sciences, University of Amsterdam, 1098 XH Amsterdam, The Netherlands; [orcid.org/0000-0001-5024-508X](https://orcid.org/0000-0001-5024-508X); Email: [j.n.h.reek@uva.nl](mailto:j.n.h.reek@uva.nl)

### Authors

Eduard O. Bobylev – van 't Hoff Institute for Molecular Sciences, University of Amsterdam, 1098 XH Amsterdam, The Netherlands

David A. Poole, III – van 't Hoff Institute for Molecular Sciences, University of Amsterdam, 1098 XH Amsterdam, The Netherlands

Bas de Bruin – van 't Hoff Institute for Molecular Sciences, University of Amsterdam, 1098 XH Amsterdam, The Netherlands; [orcid.org/0000-0002-3482-7669](https://orcid.org/0000-0002-3482-7669)

Complete contact information is available at:

<https://pubs.acs.org/doi/10.1021/jacs.2c05507>

### Notes

The authors declare no competing financial interest.

## ACKNOWLEDGMENTS

We kindly acknowledge the University of Amsterdam for financial support to RPA sustainable chemistry. We would like to thank Eline Meijer and Rens Ham for discussions.

## REFERENCES

- Ghogare, A. A.; Greer, A. Using Singlet Oxygen to Synthesize Natural Products and Drugs. *Chem. Rev.* **2016**, *116*, 9994–10034.
- Hoffmann, N. Photochemical Reactions as Key Steps in Organic Synthesis. *Chem. Rev.* **2008**, *108*, 1052–1103.
- Al-Nu'airat, J.; Oluwoye, I.; Zeinali, N.; Altarawneh, M.; Dlugogorski, B. Z. Review of Chemical Reactivity of Singlet Oxygen with Organic Fuels and Contaminants. *Chem. Rec.* **2021**, *21*, 315–342.



- (4) Castro, E.; Garcia, A. H.; Zavala, G.; Echegoyen, L. Fullerenes in Biology and Medicine. *J. Mater. Chem. B* **2017**, *5*, 6523–6535.
- (5) Di Mascio, P.; Martinez, G. R.; Miyamoto, S.; Ronsein, G. E.; Medeiros, M. H. G.; Cadet, J. Singlet Molecular Oxygen Reactions with Nucleic Acids, Lipids, and Proteins. *Chem. Rev.* **2019**, *119*, 2043–2086.
- (6) Dolmans, D. E. J. G. J.; Fukumura, D.; Jain, R. K. Photodynamic Therapy for Cancer. *Nat. Rev. Cancer* **2003**, *3*, 380–387.
- (7) Ogilby, P. R. Singlet Oxygen: There Is Indeed Something New under the Sun. *Chem. Soc. Rev.* **2010**, *39*, 3181.
- (8) DeRosa, M. Photosensitized Singlet Oxygen and Its Applications. *Coord. Chem. Rev.* **2002**, *233–234*, 351–371.
- (9) Kochevar, I. E.; Redmond, R. W. Photosensitized Production of Singlet Oxygen. *Methods Enzymol.* **2000**, *319*, 20–28.
- (10) Naranjo, A.; Arboleda, A.; Martinez, J. D.; Durkee, H.; Aguilar, M. C.; Relhan, N.; Nikpoor, N.; Galor, A.; Dubovy, S. R.; Leblanc, R.; Flynn, H. W., Jr; Miller, D.; Parel, J.-M.; Amescua, G. Rose Bengal Photodynamic Antimicrobial Therapy for Patients With Progressive Infectious Keratitis: A Pilot Clinical Study. *Am. J. Ophthalmol.* **2019**, *208*, 387–396.
- (11) Linden, S. M.; Neckers, D. C. Fundamental Properties of Rose Bengal. 25. Bleaching Studies of Rose Bengal Onium Salts. *J. Am. Chem. Soc.* **1988**, *110*, 1257–1260.
- (12) Prat, F.; Stackow, R.; Bernstein, R.; Qian, W.; Rubin, Y.; Foote, C. S. Triplet-State Properties and Singlet Oxygen Generation in a Homologous Series of Functionalized Fullerene Derivatives. *J. Phys. Chem. A* **1999**, *103*, 7230–7235.
- (13) Yamakoshi, Y.; Umezawa, N.; Ryu, A.; Arakane, K.; Miyata, N.; Goda, Y.; Masumizu, T.; Nagano, T. Active Oxygen Species Generated from Photoexcited Fullerene (C<sub>60</sub>) as Potential Medicines: O<sub>2</sub>-• versus <sup>1</sup>O<sub>2</sub>. *J. Am. Chem. Soc.* **2003**, *125*, 12803–12809.
- (14) Davis, C. M.; Lim, J. M.; Larsen, K. R.; Kim, D. S.; Sung, Y. M.; Lyons, D. M.; Lynch, V. M.; Nielsen, K. A.; Jeppesen, J. O.; Kim, D.; Park, J. S.; Sessler, J. L. Ion-Regulated Allosteric Binding of Fullerenes (C<sub>60</sub> and C<sub>70</sub>) by Tetrathiafulvalene-Calix[4]Pyrroles. *J. Am. Chem. Soc.* **2014**, *136*, 10410–10417.
- (15) Ho, K.-H. L.; Hijazi, I.; Rivier, L.; Gautier, C.; Joussembe, B.; de Miguel, G.; Romero-Nieto, C.; Guldi, D. M.; Heinrich, B.; Donnio, B.; Campidelli, S. Host-Guest Complexation of [60]Fullerenes and Porphyrins Enabled by “Click Chemistry”. *Chem.—Eur. J.* **2013**, *19*, 11374–11381.
- (16) Ke, X.-S.; Kim, T.; Brewster, J. T., II; Lynch, V. M.; Kim, D.; Sessler, J. L. Expanded Rosarin: A Versatile Fullerene (C<sub>60</sub>) Receptor. *J. Am. Chem. Soc.* **2017**, *139*, 4627–4630.
- (17) Sygula, A. Corannulene-Adorned Molecular Receptors for Fullerenes Utilizing the  $\pi$ - $\pi$  Stacking of Curved-Surface Conjugated Carbon Networks. Design, Synthesis and Testing. *Synlett* **2016**, *27*, 2070–2080.
- (18) Fuertes-Espinosa, C.; García-Simón, C.; Pujals, M.; Garcia-Borrás, M.; Gómez, L.; Parella, T.; Juanhuix, J.; Imaz, I.; Maspoch, D.; Costas, M.; Ribas, X. Supramolecular Fullerene Sponges as Catalytic Masks for Regioselective Functionalization of C<sub>60</sub>. *Chem.* **2020**, *6*, 169–186.
- (19) Martínez-Agramunt, V.; Peris, E. Photocatalytic Properties of a Palladium Metallosquare with Encapsulated Fullerenes via Singlet Oxygen Generation. *Inorg. Chem.* **2019**, *58*, 11836–11842.
- (20) Shi, Y.; Cai, K.; Xiao, H.; Liu, Z.; Zhou, J.; Shen, D.; Qiu, Y.; Guo, Q.-H.; Stern, C.; Wasielewski, M. R.; Diederich, F.; Goddard, W. A., III; Stoddart, J. F. Selective Extraction of C<sub>70</sub> by a Tetragonal Prismatic Porphyrin Cage. *J. Am. Chem. Soc.* **2018**, *140*, 13835–13842.
- (21) Brenner, W.; Ronson, T. K.; Nitschke, J. R. Separation and Selective Formation of Fullerene Adducts within an M<sup>II</sup><sub>8</sub>L<sub>6</sub> Cage. *J. Am. Chem. Soc.* **2017**, *139*, 75–78.
- (22) Chen, B.; Holstein, J. J.; Horiuchi, S.; Hiller, W. G.; Clever, G. H. Pd(II) Coordination Sphere Engineering: Pyridine Cages, Quinoline Bowls, and Heteroleptic Pills Binding One or Two Fullerenes. *J. Am. Chem. Soc.* **2019**, *141*, 8907–8913.
- (23) Fuertes-Espinosa, C.; Gómez-Torres, A.; Morales-Martínez, R.; Rodríguez-Forteza, A.; García-Simón, C.; Gándara, F.; Imaz, I.; Juanhuix, J.; Maspoch, D.; Poblet, J. M.; Echegoyen, L.; Ribas, X. Purification of Uranium-Based Endohedral Metallofullerenes (EMFs) by Selective Supramolecular Encapsulation and Release. *Angew. Chem., Int. Ed.* **2018**, *57*, 11294–11299.
- (24) Hasegawa, S.; Meichner, S. L.; Holstein, J. J.; Baksi, A.; Kasanmascheff, M.; Clever, G. H. Long-Lived C<sub>60</sub> Radical Anion Stabilized Inside an Electron-Deficient Coordination Cage. *J. Am. Chem. Soc.* **2021**, *143*, 9718–9723.
- (25) Inokuma, Y.; Arai, T.; Fujita, M. Networked Molecular Cages as Crystalline Sponges for Fullerenes and Other Guests. *Nat. Chem.* **2010**, *2*, 780–783.
- (26) Mahata, K.; Frischmann, P. D.; Würthner, F. Giant Electroactive M<sub>4</sub>L<sub>6</sub> Tetrahedral Host Self-Assembled with Fe(II) Vertices and Perylene Bisimide Dye Edges. *J. Am. Chem. Soc.* **2013**, *135*, 15656–15661.
- (27) Meng, W.; Breiner, B.; Rissanen, K.; Thoburn, J. D.; Clegg, J. K.; Nitschke, J. R. A Self-Assembled M<sub>8</sub>L<sub>6</sub> Cubic Cage That Selectively Encapsulates Large Aromatic Guests. *Angew. Chem., Int. Ed.* **2011**, *50*, 3479–3483.
- (28) Purba, P. C.; Maity, M.; Bhattacharyya, S.; Mukherjee, P. S. A Self-Assembled Palladium(II) Barrel for Binding of Fullerenes and Photosensitization Ability of the Fullerene-Encapsulated Barrel. *Angew. Chem., Int. Ed.* **2021**, *60*, 14109–14116.
- (29) Suzuki, K.; Takao, K.; Sato, S.; Fujita, M. Coronene Nanophase within Coordination Spheres: Increased Solubility of C<sub>60</sub>. *J. Am. Chem. Soc.* **2010**, *132*, 2544–2545.
- (30) García-Simón, C.; Costas, M.; Ribas, X. Metallo-supramolecular Receptors for Fullerene Binding and Release. *Chem. Soc. Rev.* **2016**, *45*, 40–62.
- (31) Rizzuto, F. J.; Nitschke, J. R. Stereochemical Plasticity Modulates Cooperative Binding in a Co<sup>II</sup><sub>12</sub>L<sub>6</sub> Cuboctahedron. *Nat. Chem.* **2017**, *9*, 903–908.
- (32) Rizzuto, F. J.; von Krbeek, L. K. S.; Nitschke, J. R. Strategies for Binding Multiple Guests in Metal–Organic Cages. *Nat. Rev. Chem.* **2019**, *3*, 204–222.
- (33) Rizzuto, F. J.; Wood, D. M.; Ronson, T. K.; Nitschke, J. R. Tuning the Redox Properties of Fullerene Clusters within a Metal–Organic Capsule. *J. Am. Chem. Soc.* **2017**, *139*, 11008–11011.
- (34) Sato, H.; Tashiro, K.; Shinmori, H.; Osuka, A.; Murata, Y.; Komatsu, K.; Aida, T. Positive Heterotropic Cooperativity for Selective Guest Binding via Electronic Communications through a Fused Zinc Porphyrin Array. *J. Am. Chem. Soc.* **2005**, *127*, 13086–13087.
- (35) Shubina, T. E.; Sharapa, D. I.; Schubert, C.; Zahn, D.; Halik, M.; Keller, P. A.; Pyne, S. G.; Jennepalli, S.; Guldi, D. M.; Clark, T. Fullerene Van Der Waals Oligomers as Electron Traps. *J. Am. Chem. Soc.* **2014**, *136*, 10890–10893.
- (36) Shanmugaraju, S.; Vajpayee, V.; Lee, S.; Chi, K.-W.; Stang, P. J.; Mukherjee, P. S. Coordination-Driven Self-Assembly of 2D-Metal-lamacrocycles Using a New Carbazole-Based Dipyrindyl Donor: Synthesis, Characterization, and C<sub>60</sub> Binding Study. *Inorg. Chem.* **2012**, *51*, 4817–4823.
- (37) Suzuki, K.; Tominaga, M.; Kawano, M.; Fujita, M. Self-Assembly of an M<sub>6</sub>L<sub>12</sub> Coordination Cube. *Chem. Commun.* **2009**, 1638.
- (38) Ashton, P. R.; Diederich, F.; Gómez-López, M.; Nierengarten, J.-F.; Preece, J. A.; Raymo, F. M.; Stoddart, J. F. Self-Assembly of the First Fullerene-Containing[2]Catenane. *Angew. Chem., Int. Ed.* **1997**, *36*, 1448–1451.
- (39) Steed, J. W.; Junk, P. C.; Atwood, J. L.; Barnes, M. J.; Raston, C. L.; Burkhalter, R. S. Ball and Socket Nanostructures: New Supramolecular Chemistry Based on Cyclotrimeratrylene. *J. Am. Chem. Soc.* **1994**, *116*, 10346–10347.
- (40) Dell’Anna, G. M.; Annunziata, R.; Benaglia, M.; Celentano, G.; Cozzi, F.; Francesconi, O.; Roelens, S. Aromatic Tripodal Receptors for (C<sub>60</sub>-Ih)[5,6]Fullerene. *Org. Biomol. Chem.* **2009**, *7*, 3871.

(41) Bobylev, E. O.; de Bruin, B.; Reek, J. N. H. Catalytic Formation of Coordination-Based Self-Assemblies by Halide Impurities. *Inorg. Chem.* **2021**, *60*, 12498–12505.

(42) Ulatowski, F.; Dąbrowa, K.; Bałakier, T.; Jurczak, J. Recognizing the Limited Applicability of Job Plots in Studying Host–Guest Interactions in Supramolecular Chemistry. *J. Org. Chem.* **2016**, *81*, 1746–1756.

(43) Poole, D. A.; Bobylev, E. O.; Mathew, S.; Reek, J. N. H. Topological Prediction of Palladium Coordination Cages. *Chem. Sci.* **2020**, *11*, 12350–12357.

(44) Martin, A. C. R. *ProFit* v3.0; UCL, 2009, [www.bioinf.org.uk/software/profit/](http://www.bioinf.org.uk/software/profit/) (accessed 2019-05-01).

(45) Kollman, P. A.; Massova, I.; Reyes, C.; Kuhn, B.; Huo, S.; Chong, L.; Lee, M.; Lee, T.; Duan, Y.; Wang, W.; Donini, O.; Cieplak, P.; Srinivasan, J.; Case, D. A.; Cheatham, T. E. Calculating Structures and Free Energies of Complex Molecules: Combining Molecular Mechanics and Continuum Models. *Acc. Chem. Res.* **2000**, *33*, 889–897.

(46) Li, M.; Jiang, S.; Zhang, Z.; Hao, X.-Q.; Jiang, X.; Yu, H.; Wang, P.; Xu, B.; Wang, M.; Tian, W. Tetraphenylethylene-Based Emissive Supramolecular Metallacages Assembled by Terpyridine Ligands. *CCS Chemistry* **2020**, *2*, 337–348.

(47) Preston, D.; Sutton, J. J.; Gordon, K. C.; Crowley, J. D. A Nona-nuclear Heterometallic Pd<sub>3</sub>Pt<sub>6</sub> “Donut”-Shaped Cage: Molecular Recognition and Photocatalysis. *Angew. Chem., Int. Ed.* **2018**, *57*, 8659–8663.

(48) Pullen, S.; Löffler, S.; Platzek, A.; Holstein, J. J.; Clever, G. H. Substrate and Product Binding inside a Stimuli-Responsive Coordination Cage Acting as a Singlet Oxygen Photosensitizer. *Dalton Trans.* **2020**, *49*, 9404–9410.

(49) Kroto, H. W.; Heath, J. R.; O’Brien, S. C.; Curl, R. F.; Smalley, R. E. C<sub>60</sub>: Buckminsterfullerene. *Nature* **1985**, *318*, 162–163.

(50) Bobylev, E. O.; Poole, D. A., III; Bruin, B.; Reek, J. N. H. How to Prepare Kinetically Stable Self-assembled Pt<sub>12</sub>L<sub>24</sub> Nanocages While Circumventing Kinetic Traps. *Chem.—Eur. J.* **2021**, *27*, 12667–12674.

(51) Yan, X.; Wei, P.; Liu, Y.; Wang, M.; Chen, C.; Zhao, J.; Li, G.; Saha, M. L.; Zhou, Z.; An, Z.; Li, X.; Stang, P. J. Endo- and Exo-Functionalized Tetraphenylethylene M<sub>12</sub>L<sub>24</sub> Nanospheres: Fluorescence Emission inside a Confined Space. *J. Am. Chem. Soc.* **2019**, *141*, 9673–9679.

(52) Sepehrpour, H.; Fu, W.; Sun, Y.; Stang, P. J. Biomedically Relevant Self-Assembled Metallacycles and Metallacages. *J. Am. Chem. Soc.* **2019**, *141*, 14005–14020.

(53) Li, Z.; Kishi, N.; Yoza, K.; Akita, M.; Yoshizawa, M. Isostructural M<sub>2</sub>L<sub>4</sub> Molecular Capsules with Anthracene Shells: Synthesis, Crystal Structures, and Fluorescent Properties. *Chem.—Eur. J.* **2012**, *18*, 8358–8365.

(54) Bobylev, E. O.; Poole, D. A., III; de Bruin, B.; Reek, J. N. H. Selective Formation of Pt<sub>12</sub>L<sub>24</sub> Nanospheres by Ligand Design. *Chem. Sci.* **2021**, *12*, 7696–7705.

(55) Baker, A.; Kanofsky, J. R. Quenching of Singlet Oxygen by Biomolecules from L1210 Leukemia Cells. *Photochem. Photobiol.* **1992**, *55*, 523–528.